NASA Contractor Report 189722
ICASE Report No. 92–57

ICASE

ON THE PREDICTION OF TURBULENT SECONDARY FLOWS

C. G. Speziale
R. M. C. So
B. A. Younis

Contract No. NAS1–19480
October 1992

Institute for Computer Applications in Science and Engineering
NASA Langley Research Center
Hampton, Virginia 23681–0001

Operated by the Universities Space Research Association

National Aeronautics and
Space Administration

Langley Research Center
Hampton, Virginia 23665-5225

ON THE PREDICTION OF TURBULENT SECONDARY FLOWS

C. G. Speziale*
ICASE, NASA Langley Research Center
Hampton, VA 23681

R. M. C. So
Arizona State University
Tempe, AZ 85287

B. A. Younis*
City University
London, England EC1V OHB

ABSTRACT

The prediction of turbulent secondary flows with Reynolds stress models in circular pipes and non-circular ducts is reviewed. Turbulence-driven secondary flows in straight non-circular ducts are considered along with turbulent secondary flows in pipes and ducts that arise from curvature or a system rotation. The physical mechanisms that generate these different kinds of secondary flows are outlined and the level of turbulence closure required to properly compute each type is discussed in detail. Illustrative computations of a variety of different secondary flows obtained from two-equation turbulence models and second-order closures are provided to amplify these points.

*This research was supported by the National Aeronautics and Space Administration under NASA Contract No. NAS1-19480 while the first and third authors were in residence at the Institute for Computer Applications in Science and Engineering (ICASE), NASA Langley Research Center, Hampton, VA 23681-0001.

1. INTRODUCTION

The turbulence structure of internal flows within circular pipes or non-circular ducts can be altered considerably by the occurrence of secondary flows [1-21]. These secondary flows lead to friction losses and can shift the location of maximum momentum transport from the pipe or duct centerline – two effects that can have profound consequences for engineering design. Consequently, there is the need for turbulence models that can reliably predict the secondary flows that occur in engineering applications which include turbomachinery impellers and blade passages, aircraft intakes, and pipe or duct cooling systems, to name a few.

In this paper, the prediction of four fundamental types of secondary flows are discussed: (1) turbulence-driven secondary flows in straight ducts of non-circular cross-section, (2) turbulent secondary flows in curved circular pipes, (3) turbulent secondary flows in curved ducts of non-circular cross-section and (4) turbulent secondary flows in rotating ducts of non-circular cross-section. These flows are selected since they involve secondary flows generated by a combination of the effects of normal Reynolds stress differences, streamline curvature and body forces arising from a system rotation. Thus, a relatively broad basis for the evaluation of models can be provided. The ability of two-equation models and second-order closures to predict these types of turbulent secondary flows will be evaluated in a systematic manner. A variety of illustrative calculations of secondary flows will be presented along with an assessment of the progress that has been made in the analysis of these flows.

2. ANALYSIS OF SECONDARY FLOWS

We will consider the mean turbulent flow of a viscous incompressible fluid. The Reynolds-averaged Navier-Stokes and continuity equations take the form

$$\frac{\partial \overline{u}_i}{\partial t} + \overline{u}_j \frac{\partial \overline{u}_i}{\partial x_j} = -\frac{\partial \overline{p}}{\partial x_i} + \nu \nabla^2 \overline{u}_i - \frac{\partial \tau_{ij}}{\partial x_j} - 2 e_{ijk} \Omega_j \overline{u}_k \tag{1}$$

$$\frac{\partial \overline{u}_i}{\partial x_i} = 0 \tag{2}$$

in a steadily rotating frame where $\overline{u}_i$ is the mean velocity, $\overline{p}$ is the modified mean pressure, Ω_i is the angular velocity of the reference frame, $\tau_{ij} \equiv \overline{u_i' u_j'}$ is the Reynolds stress tensor, and ν is the kinematic viscosity of the fluid. In (1)-(2), the Einstein summation convention applies to repeated indices and e_{ijk} denotes the permutation tensor.

First, we will consider the case of a straight circular pipe or non-circular duct whose axis lies along the z-direction and whose cross-section lies in the x, y-plane (see Figure 1). For

fully-developed turbulent flow, where $\overline{\mathbf{u}} = \overline{u}(x,y)\boldsymbol{i} + \overline{v}(x,y)\boldsymbol{j} + \overline{w}(x,y)\boldsymbol{k}$, the secondary flow $(\overline{u}, \overline{v})$ is derivable from a stream function $\overline{\psi}$:

$$\overline{u} = -\frac{\partial \overline{\psi}}{\partial y}, \quad \overline{v} = \frac{\partial \overline{\psi}}{\partial x}. \tag{3}$$

The Reynolds-averaged Navier-Stokes equations can then be solved in the alternative axial velocity/vorticity-stream function form given by

$$\overline{u}\frac{\partial \overline{w}}{\partial x} + \overline{v}\frac{\partial \overline{w}}{\partial y} = G + \nu\nabla^2\overline{w} - \frac{\partial \tau_{xz}}{\partial x} - \frac{\partial \tau_{yz}}{\partial y} + 2\Omega\overline{u} \tag{4}$$

$$\overline{u}\frac{\partial \overline{\zeta}}{\partial x} + \overline{v}\frac{\partial \overline{\zeta}}{\partial y} = \nu\nabla^2\overline{\zeta} + \frac{\partial^2(\tau_{xx} - \tau_{yy})}{\partial x \partial y} + \frac{\partial^2 \tau_{xy}}{\partial y^2} - \frac{\partial^2 \tau_{xy}}{\partial x^2} + 2\Omega\frac{\partial \overline{w}}{\partial y} \tag{5}$$

$$\nabla^2\overline{\psi} = \overline{\zeta} \tag{6}$$

where $\partial\overline{p}/\partial z \equiv -G$ is the constant applied pressure gradient driving the flow and $\overline{\zeta} \equiv \partial\overline{v}/\partial x - \partial\overline{u}/\partial y$ is the axial component of the mean vorticity vector. Here, the angular velocity $\boldsymbol{\Omega} = \Omega\boldsymbol{j}$ corresponds to a general spanwise rotation since we can align the component of the axis of rotation, that is normal to the axial direction, with the y-axis. Since the flow is fully-developed, the component of the angular velocity along the z-axis does not enter into Eqs. (4)-(5).

From (3) and (6), it is clear that secondary flows are generated by the axial mean vorticity $\overline{\zeta}$ which becomes non-zero in a straight duct or pipe only if there are *normal Reynolds stress differences* $(\tau_{yy} - \tau_{xx})$ or *Coriolis forces* $(2\Omega\partial\overline{w}/\partial y)$ arising from a spanwise rotation. In the subsections to follow we will briefly categorize secondary flows in pipes and ducts.

2.1. Straight Ducts ($\boldsymbol{\Omega} = \mathbf{o}$)

It is the axial vorticity source term

$$\Phi_\zeta = \frac{\partial^2(\tau_{xx} - \tau_{yy})}{\partial x \partial y} + \frac{\partial^2 \tau_{xy}}{\partial y^2} - \frac{\partial^2 \tau_{xy}}{\partial x^2} \tag{7}$$

that leads to the generation of turbulent secondary flows in straight non-circular ducts. A necessary condition for the occurrence of secondary flows is that the axial mean velocity $\overline{w}(x,y)$ must give rise to a non-zero normal Reynolds stress difference $\tau_{xx} - \tau_{yy}$ (otherwise, τ_{xy}, and hence Φ_ζ, will vanish; see Speziale [12,16]). For a circular pipe, even though $\tau_{xx} - \tau_{yy}$ is non-zero, $\Phi_\zeta = 0$ due to the azimuthal symmetry of the axial mean velocity; consequently no secondary flows occur [3]. For non-circular ducts, if $\tau_{xx} - \tau_{yy} \neq 0$, then invariably, Φ_ζ will

be non-zero and secondary flows are generated. From this result it is clear that any eddy viscosity model based on the Boussinesq hypothesis

$$\tau_{ij} = \frac{2}{3}K\delta_{ij} - \nu_T\left(\frac{\partial \overline{u}_i}{\partial x_j} + \frac{\partial \overline{u}_j}{\partial x_i}\right) \tag{8}$$

(where $K \equiv \frac{1}{2}\tau_{ii}$ is the turbulent kinetic energy and ν_T is the eddy viscosity) will be incapable of predicting secondary flows in a straight non-circular duct. According to (8), $\overline{\mathbf{u}} = (0, 0, \overline{w})$ yields $\tau_{yy} = \tau_{xx} = \frac{2}{3}K$ and, hence, the axial mean velocity gives rise to a vanishing normal Reynolds stress difference $\tau_{yy} - \tau_{xx}$ which violates the necessary condition for secondary flow. *Hence, anisotropic eddy viscosity models – where nonlinear strain-dependent terms are included – constitute the simplest level of Reynolds stress closure that can predict secondary flows in straight non-circular ducts.* Three examples of anisotropic eddy viscosity models are the nonlinear $K - \varepsilon$ model of Speziale [22], the two-scale DIA model of Yoshizawa [23], and the RNG based model of Rubinstein and Barton [24]. In the former model – for which sample computations will be presented in the next section – the Reynolds stress is represented as follows:

$$\tau_{ij} = \frac{2}{3}K\delta_{ij} - 2C_\mu\frac{K^2}{\varepsilon}\overline{S}_{ij} - 4C_D C_\mu^2\frac{K^3}{\varepsilon^2}\left(\overset{\circ}{\overline{S}}_{ij} + \overline{S}_{ik}\overline{S}_{kj} + \frac{1}{3}\overline{S}_{k\ell}\overline{S}_{k\ell}\delta_{ij}\right) \tag{9}$$

where

$$\overset{\circ}{\overline{S}}_{ij} = \frac{\partial \overline{S}_{ij}}{\partial t} + \overline{u}_k\frac{\partial \overline{S}_{ij}}{\partial x_k} - \frac{\partial \overline{u}_i}{\partial x_k}\overline{S}_{kj} - \frac{\partial \overline{u}_j}{\partial x_k}\overline{S}_{ki} \tag{10}$$

is the frame-indifferent Oldroyd derivative of the mean rate of strain tensor $\overline{S}_{ij} \equiv \frac{1}{2}(\partial \overline{u}_i/\partial x_j + \partial \overline{u}_j/\partial x_i)$ and ε is the turbulent dissipation rate; $C_\mu = 0.09$ and $C_D = 1.68$ are empirical constants. In the limit as $C_D \to 0$, the eddy viscosity relation of the standard $K - \varepsilon$ model is recovered. It can be shown that in fully-developed duct flow, the axial mean velocity $\overline{w}$ gives rise to the non-zero normal Reynolds stress difference $\tau_{yy} - \tau_{xx} = C_D C_\mu^2(K^3/\varepsilon^2)[(\partial \overline{w}/\partial x)^2 - (\partial \overline{w}/\partial y)^2]$ in (9). Hence, secondary flows are generated by the nonlinear $K - \varepsilon$ model.

For developing secondary flows, where history effects are important, a full Reynolds stress closure is needed for a more complete description. Second-order closures are based on the Reynolds stress transport equation [25]:

$$\begin{aligned}\frac{\partial \tau_{ij}}{\partial t} + \overline{u}_k\frac{\partial \tau_{ij}}{\partial x_k} &= -\tau_{ik}\frac{\partial \overline{u}_j}{\partial x_k} - \tau_{jk}\frac{\partial \overline{u}_i}{\partial x_k} + \Pi_{ij} - \frac{2}{3}\varepsilon\delta_{ij} \\ &\quad + \mathcal{D}_{ij}^T + \nu\nabla^2\tau_{ij} - 2\Omega_m(e_{mkj}\tau_{ik} + e_{mki}\tau_{jk})\end{aligned} \tag{11}$$

where Π_{ij} is the combination of the pressure-strain correlation and the deviatoric part of the dissipation rate tensor whereas $\mathcal{D}_{ij}^T$ is the turbulent transport term (here, $\boldsymbol{\Omega} = 0$ for a stationary duct). From (11), it is straightforward to show – by substituting $\overline{\mathbf{u}} = (0, 0, \overline{w})$

into this equation – that secondary flows are generated by Π_{ij} and $\mathcal{D}_{ij}^{T}$ which are the only terms that yield a normal Reynolds stress difference $\tau_{yy} - \tau_{xx}$ (see Speziale [12,16]). An order of magnitude analysis, at high Reynolds numbers, tends to indicate that anisotropies in the pressure-strain correlation are predominantly responsible for the generation of secondary flows; anisotropies in the turbulent dissipation rate and turbulent transport term appear to play a smaller role.

2.2. Rotating Pipes and Ducts

In a rotating circular pipe, the axial mean velocity $\overline{w}(r)$ gives rise to a vanishing Φ_ζ by symmetry arguments; hence, secondary flows are generated by the Coriolis term $2\Omega\partial\overline{w}/\partial y$ alone (the normal Reynolds stress differences in Φ_ζ only have an indirect effect in determining the structure of the resulting fully-developed secondary flow). Since the secondary flows in rotating circular pipes are generated exclusively by Coriolis forces, eddy viscosity models such as the $K - \varepsilon$ model are capable of describing this effect [9], albeit after some modifications. For more detailed descriptions of the flow – or for the developing flow case – either anisotropic eddy viscosity models or second-order closures should be used.

Secondary flows in rotating non-circular ducts are generated by two sources: normal Reynolds stress differences embodied in the term Φ_ζ and Coriolis forces represented by the term $2\Omega\partial\overline{w}/\partial y$. Hence, the simplest models that will yield acceptable predictions of this flow are two-equation models with an anisotropic eddy viscosity. However, since the Coriolis forces have a direct effect on the evolution of the Reynolds stresses (see Eq. (11)), second-order closure models are needed for a more complete description of this flow. Even in the absence of secondary flows, the Coriolis forces in (11) cause the axial mean velocity profiles to become asymmetric – an effect that is difficult to describe with two-equation models.

2.3. Curved Pipes and Ducts

Secondary flows in curved pipes and ducts are generated by centrifugal forces. This can be easily seen for the case of fully-developed curved duct flow with the streamwise mean velocity $\overline{w}$ and secondary flow $\overline{u}, \overline{v}$ (corresponding to the directions θ, r, and z, respectively). Here, the mean flow equations can be written in the form:

$$\overline{u}\frac{\partial\overline{w}}{\partial r} + \overline{v}\frac{\partial\overline{w}}{\partial z} + \frac{\overline{u}\,\overline{w}}{r} = G + \nu\left(\nabla^2\overline{w} - \frac{\overline{w}}{r^2}\right) - \frac{1}{r}\frac{\partial}{\partial r}(r\tau_{r\theta}) - \frac{\partial\tau_{z\theta}}{\partial z} - \frac{\tau_{r\theta}}{r} \qquad (12)$$

$$\overline{u}\frac{\partial\overline{\zeta}}{\partial r}+\overline{v}\frac{\partial\overline{\zeta}}{\partial z} = \frac{\overline{u}}{r}\overline{\zeta}+2\frac{\overline{w}}{r}\frac{\partial\overline{w}}{\partial z}+\nu\left(\nabla^2\overline{\zeta}-\frac{\overline{\zeta}}{r^2}\right)+\frac{\partial^2}{\partial r\partial z}(\tau_{zz}-\tau_{rr}) \tag{13}$$
$$+\frac{1}{r}\frac{\partial}{\partial z}(\tau_{\theta\theta}-\tau_{rr})+\frac{\partial}{\partial r}\left[\frac{1}{r}\frac{\partial}{\partial r}(r\tau_{rz})\right]-\frac{\partial^2\tau_{rz}}{\partial z^2}$$

$$\frac{\partial^2\overline{\psi}}{\partial r^2}-\frac{1}{r}\frac{\partial\overline{\psi}}{\partial r}+\frac{\partial^2\overline{\psi}}{\partial z^2}=r\overline{\zeta} \tag{14}$$

$$\overline{u}=\frac{1}{r}\frac{\partial\overline{\psi}}{\partial z},\quad \overline{v}=-\frac{1}{r}\frac{\partial\overline{\psi}}{\partial r} \tag{15}$$

where $\overline{\zeta}\equiv(\boldsymbol{\nabla}\times\overline{\mathbf{u}})_\theta=\partial\overline{u}/\partial z-\partial\overline{v}/\partial r$ is the streamwise mean vorticity, $\overline{\psi}$ is the secondary flow stream function, and $-G$ is the applied mean pressure gradient. It is clear from (13) that the streamwise vorticity source term $(2\overline{w}/r)\partial\overline{w}/\partial z$ – which constitutes a centrifugal acceleration term generated by the primary flow $\overline{w}$ – is the main generator of secondary flows in curved pipes. In curved non-circular ducts, secondary flows are generated by centrifugal effects as well as by the normal Reynolds stress differences $\tau_{zz}-\tau_{rr}$ and $\tau_{\theta\theta}-\tau_{rr}$ which play a crucial role when the curvature is weak. Consequently, two-equation models with an isotropic eddy viscosity, such as the $K-\varepsilon$ model, have yielded reasonably acceptable predictions for fully-developed secondary flows in curved pipes and curved ducts with moderate to strong curvature ratios [17]. In order to analyze curved duct flows for a range of curvature ratios, or under developing conditions, anisotropic eddy viscosity models or second-order closure models, respectively, are needed.

3. ILLUSTRATIVE EXAMPLES

We will first present computations of fully-developed turbulent flow in a straight rectangular duct (see Figure 1). A secondary flow with eight counter-rotating vortices is generated by normal Reynolds stress differences. Since the flow is fully-developed, a two-equation model with an anisotropic eddy viscosity – solved in conjunction with wall functions – suffices. In Figure 2, the mean secondary flow streamlines predicted by the nonlinear $K-\varepsilon$ model (9) at high Reynolds numbers are shown for a square duct. This secondary flow is of the order of 1-2% of the axial mean velocity. The characteristic eight-vortex secondary flow illustrated in the schematic provided in Figure 1 is reproduced. These results stand in sharp contrast to those obtained from the standard $K-\varepsilon$ model which erroneously predicts a unidirectional mean turbulent flow – a deficiency that arises from the use of an eddy viscosity model based on the Boussinesq hypothesis (8).

More quantitative comparisons will now be made for a straight 3×1 rectangular duct. The secondary flow streamlines and contours of the normal Reynolds stress anisotropy $\tau_{xx}-\tau_{yy}$

predicted by the nonlinear $K-\varepsilon$ model are compared with the experimental data of Hoagland [1] in Figures 3(a)-3(b). These results are of a comparable level of quality as those obtained from a second-order closure model similar to that of Launder, Reece and Rodi [25] as shown in Figures 4(a)-4(b). Hence, it is clear that two-equation turbulence models with an anisotropic eddy viscosity yield acceptable predictions for fully-developed secondary flows in a straight rectangular duct. For developing turbulent flows in non-circular ducts, second-order closure models yield more complete predictions [26].

The fully-developed secondary flow in a curved square duct predicted by the nonlinear $K-\varepsilon$ model at high Reynolds numbers is shown in Figures 5(a)-5(b) for two different curvature ratios C_r (i.e., the ratio of the radius of curvature to the duct width). For moderate curvature, there is a double-vortex secondary flow that undergoes a bifurcation to a four-vortex secondary flow when the curvature ratio $C_r \approx 40$. This is analogous to the Görtler instability in curved channel flow [27]. For extremely weak curvature ($C_r > 10^3$), the double-vortex secondary flow generated by centrifugal effects interacts with the eight-vortex secondary flow generated by normal Reynolds stress differences yielding an extremely complex secondary flow pattern which we will not show herein (see Hur et al. [20] and Hur [28] for more details). An anisotropic eddy viscosity model is the simplest type of model that can describe the full range of curvature ratios. For a more complete description of the flow – especially under developing conditions – second-order closure models are preferable. However, it is interesting to note that reasonably acceptable mean flow predictions have been obtained for fully-developed curved pipe flow using the standard $K-\varepsilon$ model for a limited range of curvature ratios [5].

Now, we will discuss the prediction of curved turbulent pipe flows that are not fully-developed, namely, the case of a circular pipe U-bend. Here, both history and near-wall effects play a role; consequently, a second-order closure with a near-wall turbulence model constitutes the preferred approach. We will show some illustrative computations for the Launder, Reece and Rodi model with the near wall turbulence model of Lai and So [29]. In Figures 6(a)-6(b), the computed secondary flow and mean velocity profiles along the pipe centerline (AA) and vertical radius (BB) are shown to compare favorably with the experimental data of Anwer et al. [19] for a location 67.5° into the U-bend. At this same location ($\theta = 67.5°$), the secondary flow field predicted by the full second-order closure model is compared with its counterpart obtained from the $K-\varepsilon$ model in Figures 7(a)-7(b). It is clear from these results that the second-order closure yields a more detailed picture of the secondary flow structure. Unlike the $K-\varepsilon$ model, the second-order closure model is able to predict the presence of a small subsidiary secondary flow cell near the outer bend of the pipe (see the lower left-hand corner of Figure 7(a)). The existence of this secondary flow cell has

been extrapolated from experiments [21].

Finally, we will present some computed results for fully-developed turbulent flow in rectangular ducts subjected to a spanwise rotation (i.e., the duct configuration shown in Figure 1 mounted in a frame that is rotating steadily about the y-axis with an angular velocity Ω). In a low-aspect-ratio duct, for weak to moderate rotations, secondary flows occur that are qualitatively very similar to those obtained in curved rectangular ducts (see Figures 5(a)-5(b)). For the sake of brevity, we will not show these double-vortex and four-vortex secondary flow solutions (see Younis [30]). For a large-aspect-ratio rectangular duct – which is used to experimentally simulate channel flow – a roll instability can occur at intermediate rotation rates. This is illustrated in Figure 8 which shows the appearance of counter-rotating Taylor vortices in the interior of the duct computed using a nonlinear algebraic Reynolds stress model for a rotation number (i.e., angular velocity normalized by the channel thickness and bulk mean velocity) $Ro \approx 0.1$. These Taylor cells will cause the axial mean velocity along the duct centerline (which is used to approximate channel flow) to become *asymmetric*. Such an asymmetry also arises in the absence of secondary flows due to the direct effect of Coriolis forces on the Reynolds stresses as given in Eq. (11).

One-dimensional mean velocity calculations of rotating channel flow obtained using the SSG second-order closure model [31] with wall functions are compared with experiments [32] in Figures 9(a)-9(b). At weak rotation rates (see Figure 9(a)) the second-order closure model does a reasonably good job of predicting the asymmetry in the mean velocity profile. However, as the rotation number Ro becomes of the order of 10^{-1}, the quantitative accuracy of the results degrade (see Figure 9(b) and also the results of Launder et al. [33]). This could be partially due to the neglect of roll instabilities which have been documented experimentally [8]. Full second-order closure model calculations of a rotating rectangular duct of large-aspect ratio – as illustrated in Figure 8 – should be conducted to resolve this issue. No such detailed calculations of roll-instabilities in rotating turbulent channel flow have yet to be undertaken with a second-order closure.

4. CONCLUDING REMARKS

A broad overview of turbulent secondary flows in pipes and ducts has been presented which highlights the underlying physical mechanisms responsible for their generation and the predictive capabilities of Reynolds stress models in describing these flows. Secondary flows arising from normal Reynolds stress differences, curvature, and a system rotation have been considered in an effort to establish a sufficiently general basis for the evaluation of models. In the opinion of the authors, two-equation models with an anisotropic eddy viscosity represent the simplest level of model that can predict a wide range of these flows without the ad hoc

adjustment of constants or the ad hoc prescription of turbulent length and time scales. These two-equation models do a reasonably good job of predicting turbulent secondary flows in their fully-developed state. For a more complete description of these flows – particularly under developing conditions where history effects or body forces play a significant role – second-order closures, with an asymptotically consistent near-wall turbulence model, are preferred. While future research is still needed, the results presented in this paper demonstrate the considerable progress that has been made during the past two decades in the prediction of turbulent secondary flows.

REFERENCES

1. L. C. Hoagland, *Ph.D. Thesis*, Massachusetts Institute of Technology (1960).

2. E. Brundrett and W. Baines, *J. Fluid Mech.* **19** (1964), 375.

3. F. B. Gessner and J. B. Jones, *J. Fluid Mech.* **23** (1965), 689.

4. B. E. Launder and Y. M. Ying, *J. Fluid Mech.* **54** (1972), 289.

5. S. V. Patankar, V. S. Pratap and D. B. Spalding, *J. Fluid Mech.* **62** (1974), 539.

6. F. B. Gessner and J. K. Po, *ASME J. Fluids Engng.* **98** (1976), 269.

7. A. Melling and J. H. Whitelaw, *J. Fluid Mech.* **78** (1976), 289.

8. D. K. Lezius and J. P. Johnston, *J. Fluid Mech.* **77** (1976), 153.

9. A. K. Majumdar, V. S. Pratap and D. B. Spalding, *ASME J. Fluids Engng.* **99** (1977), 148.

10. J. H. Howard, S. V. Patankar and R. M. Bordynuik, *ASME J. Fluids Engng.* **102** (1980), 456.

11. J. A. C. Humphrey, J. H. Whitelaw and G. Yee, *J. Fluid Mech.* **103** (1981), 443.

12. C. G. Speziale, *Int. J. Engng. Sci.* **20** (1982), 863.

13. S. M. Chang, J. A. C. Humphrey and A. Modavi, *Physico-Chem. Hydro.* **4** (1983), 243.

14. A. O. Demuren and W. Rodi, *J. Fluid Mech.* **140** (1984), 189.

15. J. Azzola, J. A. C. Humphrey, H. Iacovides and B. E. Launder, *ASME J. Fluids Engng.* **108** (1986), 214.

16. C. G. Speziale, *ASME J. Fluids Engng.* **108** (1986), 118.

17. P. Bradshaw, *Ann. Rev. Fluid Mech.* **19** (1987), 53.

18. Y. D. Choi, H. Iacovides and B. E. Launder, *ASME J. Fluids Engng.* **111** (1989), 59.

19. M. Anwer, R. M. C. So and Y. G. Lai, *Phys. Fluids A* **1** (1989), 1387.

20. N. Hur, S. Thangam and C. G. Speziale, *ASME J. Fluids Engng.* **112** (1990), 205.

21. Y. G. Lai, R. M. C. So and H. S. Zhang, *Theoret. Comput. Fluid Dyn.* **3** (1991), 163.

22. C. G. Speziale, *J. Fluid Mech.* **178** (1987), 459.

23. A. Yoshizawa, *Phys. Fluids* **27** (1984), 1377.

24. R. Rubinstein and J. M. Barton, *Phys. Fluids A* **2** (1990), 1472.

25. B. E. Launder, G. J. Reece and W. Rodi, *J. Fluid Mech.* **68** (1975), 537.

26. F. B. Gessner and A. F. Emery, *ASME J. Fluids Engng.* **103** (1981), 445.

27. H. Schlichting, *Boundary Layer Theory*, McGraw-Hill (1968).

28. N. Hur, *Ph.D. Thesis*, Stevens Institute of Technology (1988).

29. Y. G. Lai and R. M. C. So, *J. Fluid Mech.* **221** (1990), 641.

30. B. A. Younis, *ASME J. Fluids Engng.*, to appear.

31. C. G. Speziale, S. Sarkar and T. B. Gatski, *J. Fluid Mech.* **227** (1991), 245.

32. J. P. Johnston, R. M. Halleen and D. K. Lezius, *J. Fluid Mech.* **56** (1972), 533.

33. B. E. Launder, D. P. Tselepidakis and B. A. Younis, *J. Fluid Mech.* **183** (1987), 63.

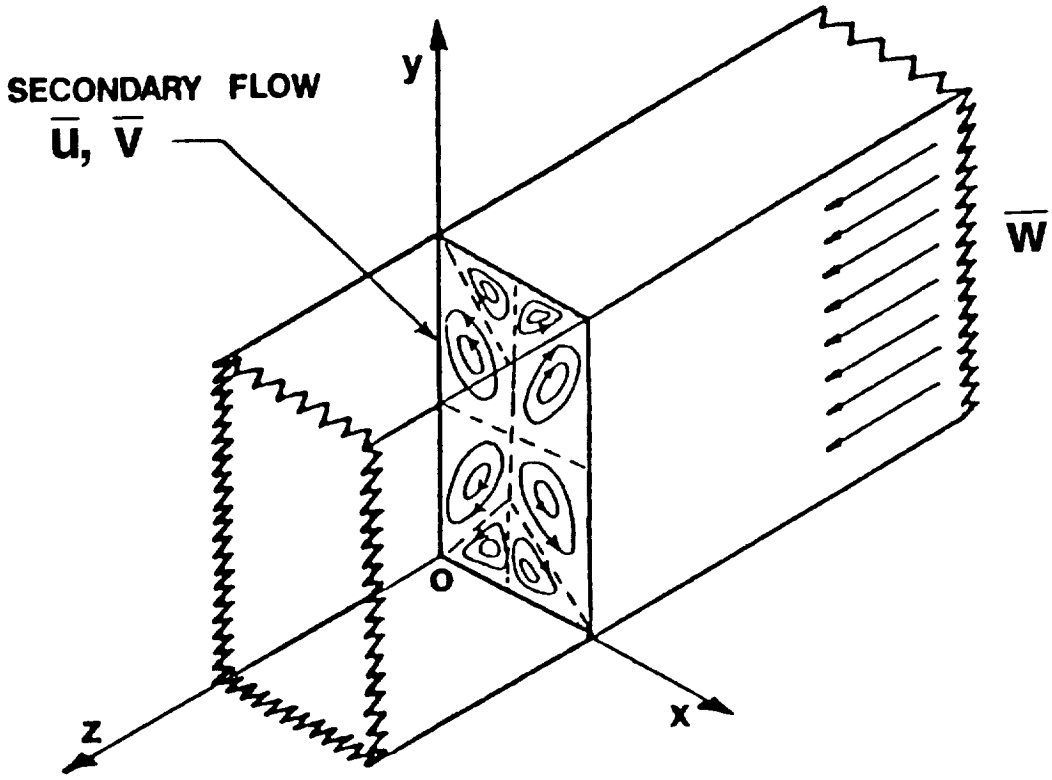

Figure 1. Schematic of turbulent secondary flow in a straight rectangular duct.

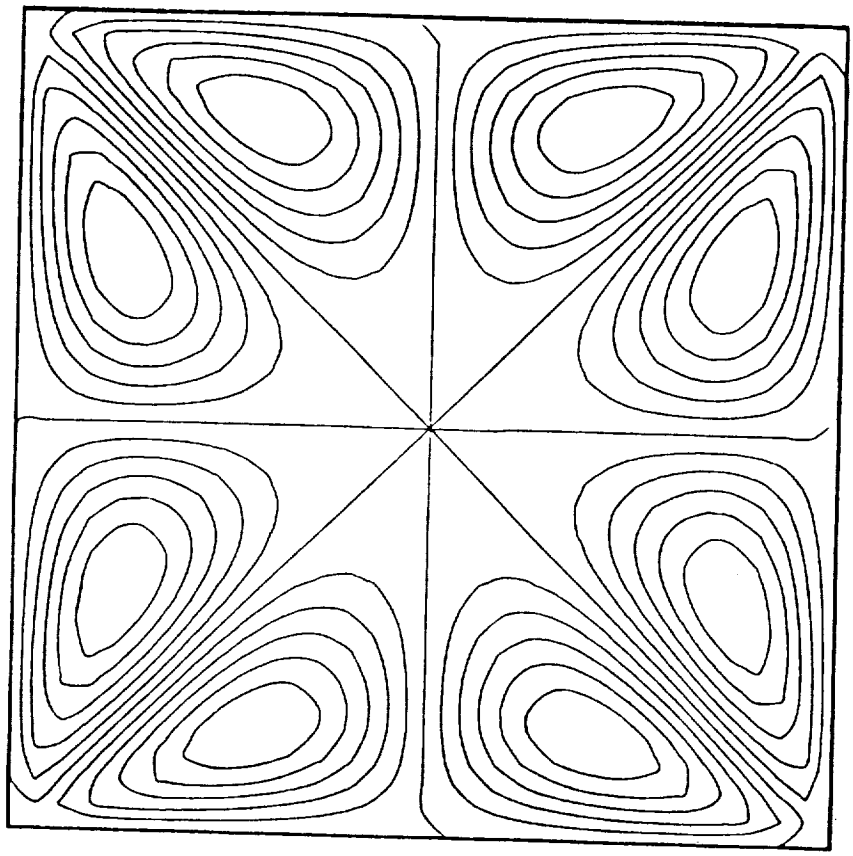

Figure 2. Secondary flow streamlines in a square duct obtained from the nonlinear $K - \varepsilon$ model.

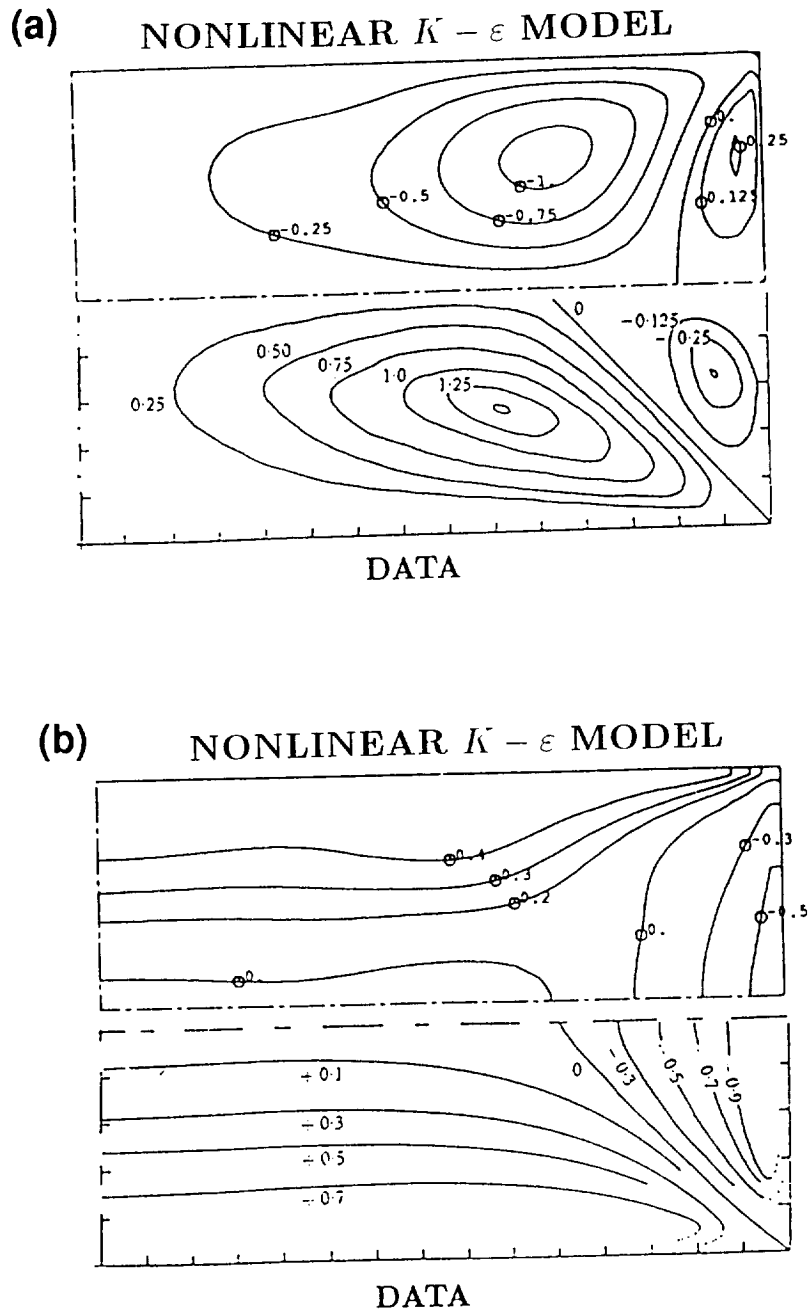

Figure 3. Comparison of the predictions of the nonlinear $K-\varepsilon$ model with the experimental data of Hoagland [1] for 3×1 rectangular duct: (a) secondary flow streamlines and (b) contours of the normal Reynolds stress difference $\tau_{xx} - \tau_{yy}$.

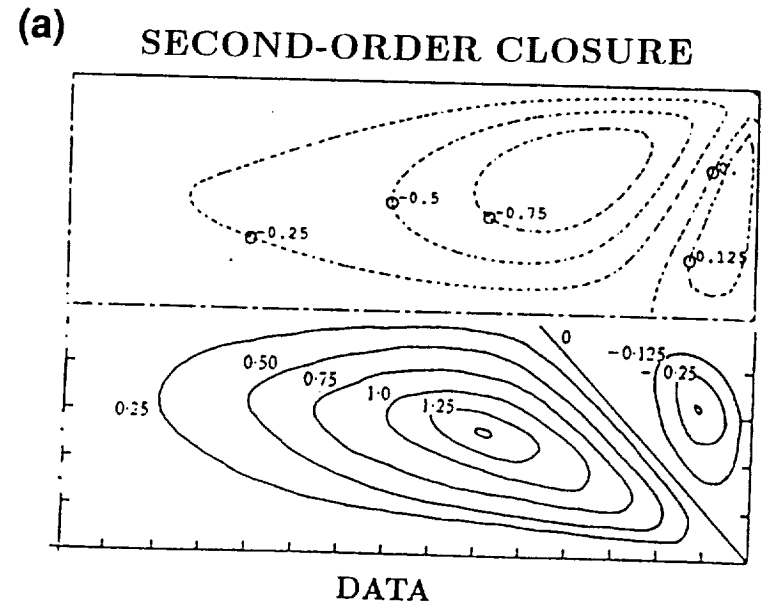

Figure 4. Comparison of the predictions of a second-order closure model with the experimental data of Hoagland [1] for a 3×1 rectangular duct: (a) secondary flow streamlines and (b) contours of the normal Reynolds stress difference $\tau_{xx} - \tau_{yy}$.

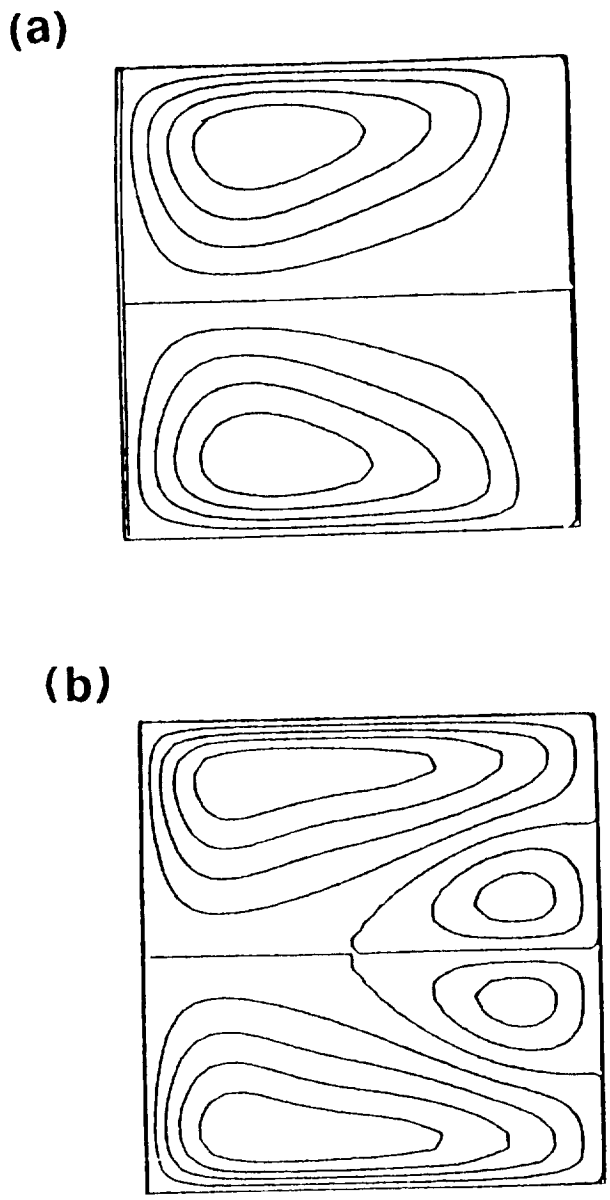

Figure 5. Computed secondary flow streamlines obtained from the nonlinear $K-\varepsilon$ model for fully-developed turbulent flow in a curved square duct: (a) $C_r = 125$ and (b) $C_r = 31.3$.

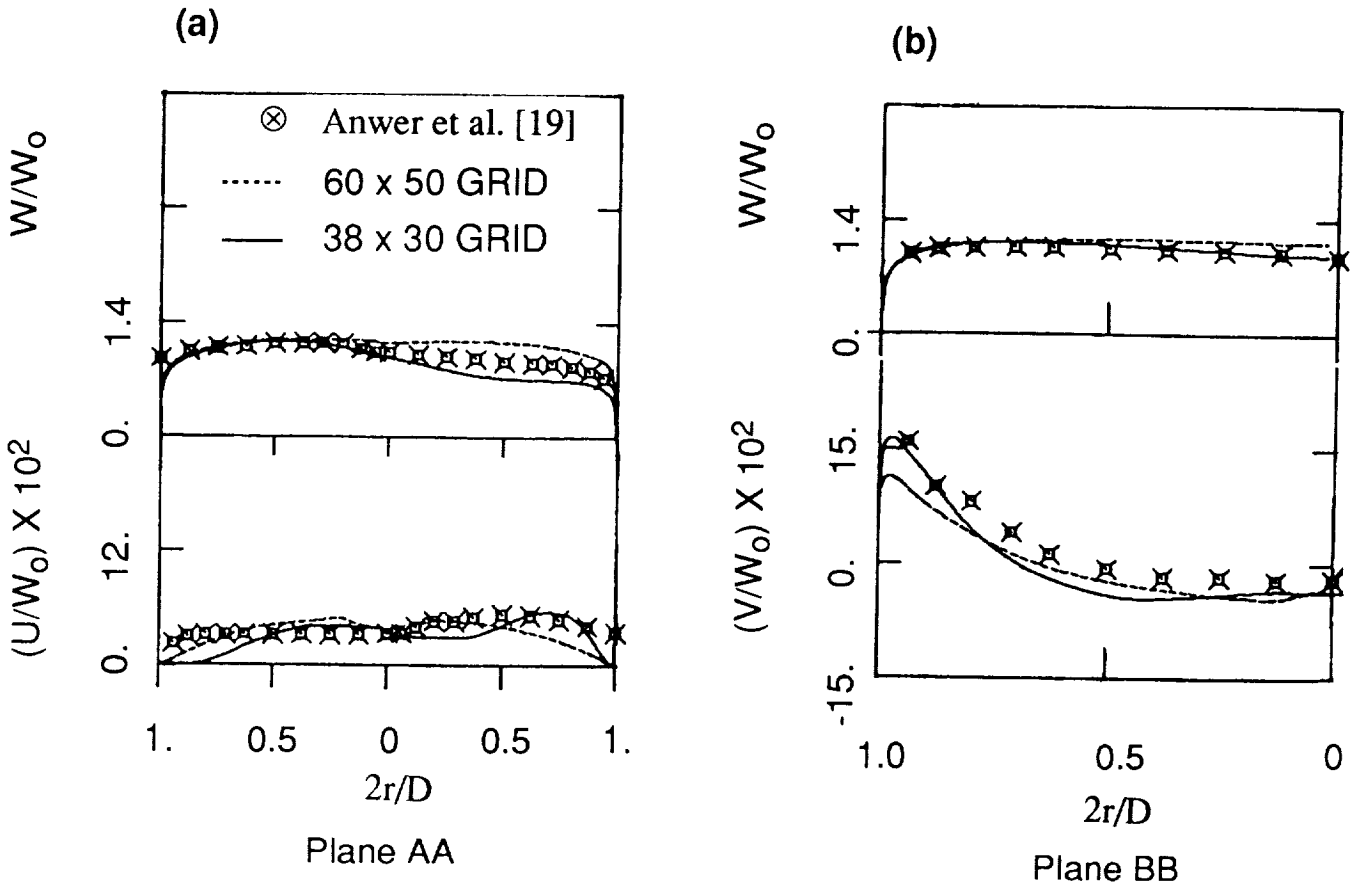

Figure 6. Comparison of the mean velocity predictions of the second-order closure model of Lai and So [29] with experimental data [19] for a circular pipe U-bend ($\theta = 67.5°$): (a) profiles along the pipe centerline (AA) and (b) profiles along the vertical radius (BB).

(a)

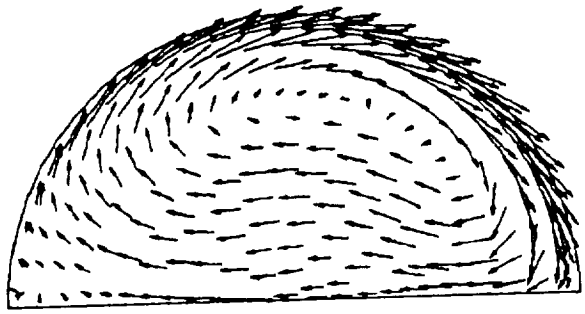

(b)

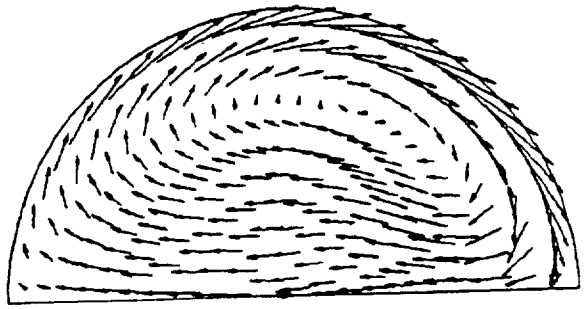

Figure 7. Computed secondary flow patterns for a circular pipe U-bend ($\theta = 67.5°$): (a) second-order closure of Lai and So [29] and (b) $K - \varepsilon$ model.

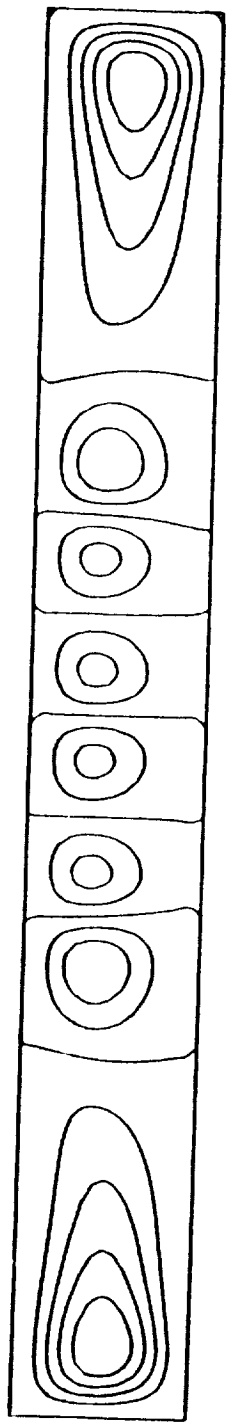

Figure 8. Secondary flow streamlines in a rotating 8×1 rectangular duct obtained using a nonlinear algebraic Reynolds stress model.

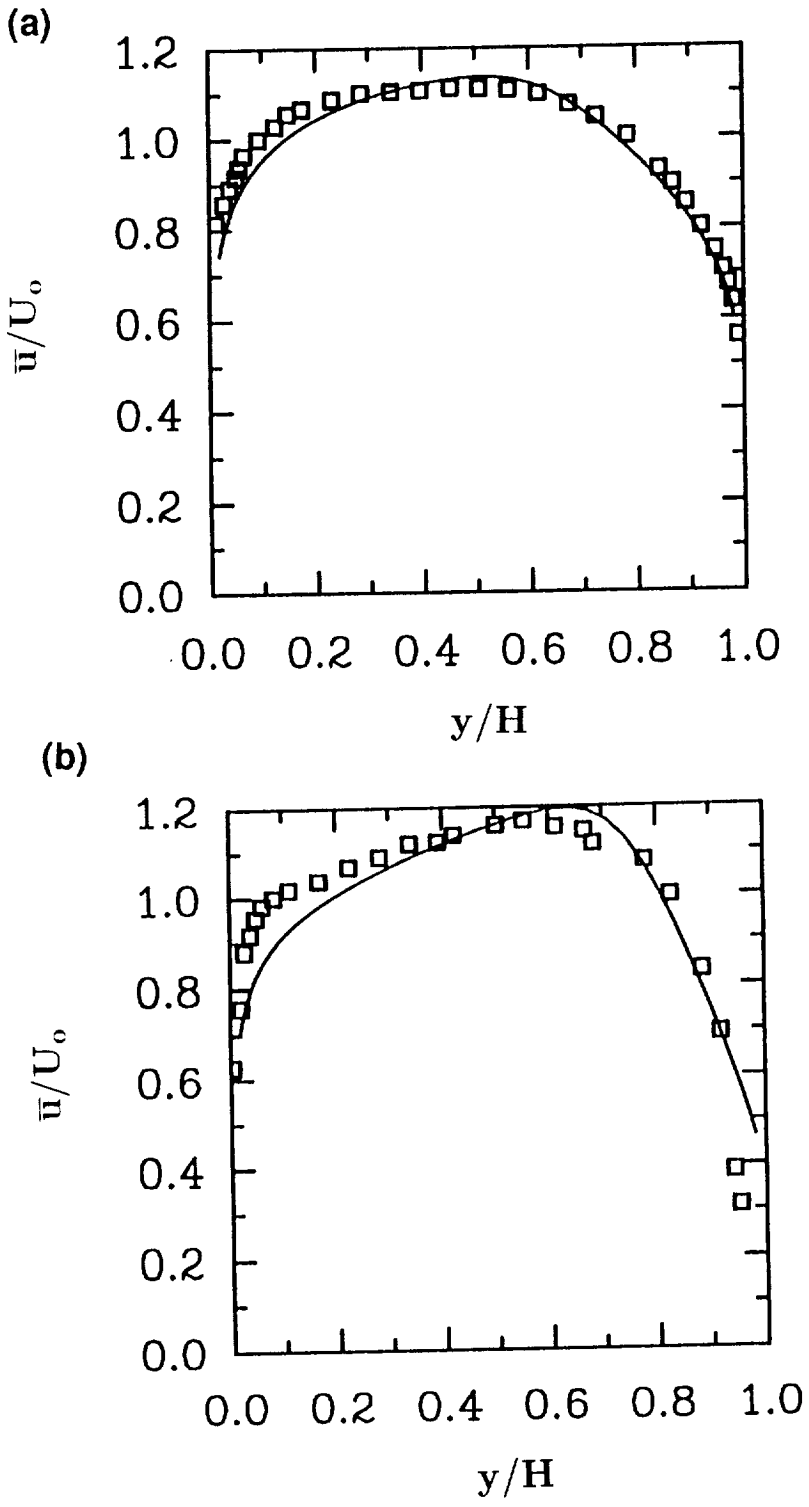

Figure 9. Comparison of the mean velocity profiles in rotating channel flow. (— SSG second-order closure model; □ Experimental data [32]): (a) $Ro = 0.068$, $Re = 35,000$ and (b) $Ro = 0.21$, $Re = 11,500$.

REPORT DOCUMENTATION PAGE

Form Approved
OMB No. 0704-0188

1. AGENCY USE ONLY (Leave blank)	2. REPORT DATE	3. REPORT TYPE AND DATES COVERED
	October 1992	Contractor Report

4. TITLE AND SUBTITLE
ON THE PREDICTION OF TURBULENT SECONDARY FLOWS

5. FUNDING NUMBERS
C NAS1-19480
WU 505-90-52-01

6. AUTHOR(S)
C.G. Speziale
R.M.C. So
B.A. Younis

7. PERFORMING ORGANIZATION NAME(S) AND ADDRESS(ES)
Institute for Computer Applications in Science and Engineering
Mail Stop 132C, NASA Langley Research Center
Hampton, VA 23681-0001

8. PERFORMING ORGANIZATION REPORT NUMBER
ICASE Report No. 92-57

9. SPONSORING / MONITORING AGENCY NAME(S) AND ADDRESS(ES)
National Aeronautics and Space Administration
Langley Research Center
Hampton, VA 23681-0001

10. SPONSORING / MONITORING AGENCY REPORT NUMBER
NASA CR-189722
ICASE Report No. 92-57

11. SUPPLEMENTARY NOTES
Langley Technical Monitor: Michael F. Card
Final Report
To appear in Near-Wall Turbulent Flows, Elsevier Press

12a. DISTRIBUTION / AVAILABILITY STATEMENT
Unclassified - Unlimited

Subject Category 34

12b. DISTRIBUTION CODE

13. ABSTRACT *(Maximum 200 words)*

The prediction of turbulent secondary flows with Reynolds stress models in circular pipes and non-circular ducts is reviewed. Turbulence-driven secondary flows in straight non-circular ducts are considered along with turbulent secondary flows in pipes and ducts that arise from curvature or a system rotation. The physical mechanisms that generate these different kinds of secondary flows are outlined and the level of turbulence closure required to properly compute each type is discussed in detail. Illustrative computations of a variety of different secondary flows obtained from two-equation turbulence models and second-order closures are provided to amplify these points.

14. SUBJECT TERMS	15. NUMBER OF PAGES
secondary flows; Reynolds stress closures; K-ε model ; curvature and rotation	21
	16. PRICE CODE A03

17. SECURITY CLASSIFICATION OF REPORT	18. SECURITY CLASSIFICATION OF THIS PAGE	19. SECURITY CLASSIFICATION OF ABSTRACT	20. LIMITATION OF ABSTRACT
Unclassified	Unclassified		